Soft Matter

Accepted Manuscript

ROYAL SOCIETY OF CHEMISTRY

www.rsc.org/softmatter

Kinetic aspects of the adsorption of xyloglucan onto cellulose nanocrystals

Ana Villares, Céline Moreau, Abir Dammak, Isabelle Capron, Bernard Cathala*

UR1268 Biopolymères Interactions Assemblages, INRA, F-44316 Nantes, France

Corresponding author at: UR1268 Biopolymères Interactions Assemblages, INRA, F-44316 Nantes, France. E-mail: Ana.Villares-Garicochea@nantes.inra.fr; Tel.: +33 240675018.

Table of content

Kinetic studies of XG adsorption onto CNC surfaces reveal two adsorption regimes: adsorption as trains at low XG concentration, or as loops and tails at high XG concentration.

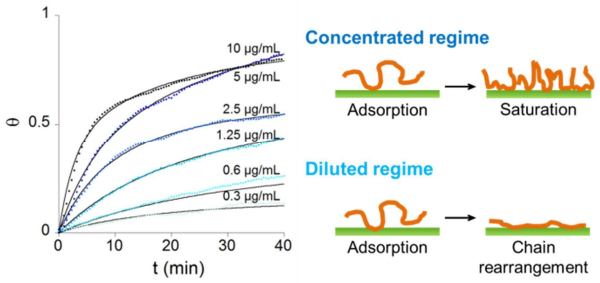

ABSTRACT

In this work, adsorption of a neutral flexible polysaccharide, xyloglucan (XG), onto thin cellulose nanocrystals (CNC) surfaces has been investigated to get more insight into the CNC-XG association. Gold-coated quartz crystals were spin-coated with one layer of CNC, and XG adsorption was monitored *in situ* by quartz crystal microbalance with dissipation (QCM-D). The adsorption of XG under flow at different concentrations did not result in the same surface concentration, which evidenced a kinetically-controlled process. In an attempt to describe the binding of XG to CNC, adsorption data were fitted to a kinetic model comprising a contribution from XG adsorption onto uncovered CNC surfaces and a contribution from XG adsorption after rearrangement. Kinetic studies evidenced the presence of two adsorption regimes as a function of XG concentration. For low XG concentrations, the kinetic constant for chain rearrangement is comparable to the kinetic constant for adsorption. This fact implies a rearrangement and alignment of XG molecules on CNC. Differently, for higher XG concentrations, the kinetic constant related to the conformational rearrangement decreases, indicating that XG molecules have no time to laterally rearrange before new XG molecules adsorb.

Keywords: Adsorption isotherm, Adsorption kinetics, Diffusion coefficient, Quartz Crystal Microbalance with Dissipation, Polysaccharides.

Introduction

Polysaccharides have arisen as potential candidates for the design and preparation of new biosourced and environmentally friendly nanomaterials.[1] Cellulose, the most abundant biopolymer on earth, has been widely exploited due to the excellent functionalities of nanocelluloses, such as surface properties,[2, 3] high mechanical performance,[4, 5] barrier properties,[6] or thermal stability,[7] among others. In nature, cellulose occurs as fibrillate structures consisting of a crystalline core and less organized (amorphous) regions linked together and arranged periodically along the microfibrils. The non-ordered domains can be hydrolyzed while the crystalline regions remain intact so as to isolate the stiff, rod-like nanocrystals. Surface modification of polysaccharides is a known approach for preserving the bulk properties of the underlying material while introducing the functionality at the surface and enabling the fabrication of multilayer architectures. In this field, adsorption of polymers onto cellulose has led to the fabrication of a wide range of assemblies. Different nanoparticles or polymers including naturally occurring polysaccharides have been adsorbed onto cellulose nanocrystals (CNC) to form ordered nanostructures. For instance, multilayers of CNC and synthetic polymers have been constructed by the layer-by-layer approach,[8] as well as hybrid films containing inorganic species such as carbon nanotubes.[9] Entirely biosourced assemblies have been also fabricated with CNC and natural polysaccharides including hemicelluloses,[10-12] lignin,[13] and chitin or chitosan derivatives.[14, 15]

Xyloglucan (XG) is one of the most common hemicelluloses occurring in plants. Its structure consists of a β-(1-4)-linked D-glucopyranosyl linear backbone with three α-(1-6)-linked xylose units, which can be substituted with β-(1-2)-linked galactosyl residues and in some cases further with arabinosyl or fucosyl residues.[16] In nature, cellulose microfibers are embedded within a network of hemicelluloses and pectins forming the primary plant cell wall. This naturally occurring assembly has shown excellent properties such as mechanical, which

has encouraged much research aimed at mimicking these architectures and fabricating thin coatings and multilayer films of cellulose and XG.[10, 17, 18] Hence, xyloglucan cultured with bacterial cellulose has demonstrated to reduce the Young's modulus and increase the extensibility of the film.[19, 20] In addition, CNC-XG assemblies develop structural colors at a certain thickness; thus, CNC-XG multilayer films have been used as a screening test for biomass-hydrolyzing enzyme detection.[11] The nature of interactions between cellulose and xyloglucan is still controversial but it is accepted that this association is established by van der Waals interactions and hydrogen bonds between polymer chains.[21]

The aim of the present study is to investigate the adsorption behavior of XG molecules on CNC deposited onto solid substrates as model surfaces mimicking naturally occurring polysaccharide architectures. Differently from suspensions in aqueous media, solid CNC layers provide conformational constraints similarly to natural composites of cellulose. An understanding of interactions between nanocrystal solid surfaces and XG is essential not only for designing new materials, but also for getting more insight into the organization and function of biopolymers in nature. CNC layer was constructed using the spin-coating assisted procedure, and layer morphology, topography, roughness, and thickness were firstly characterized by microscopy (AFM and TEM) and ellipsometry techniques. Furthermore, *in situ* adsorption monitored by QCM-D was used to probe the adsorbed water and the dissipation capacity of the CNC layer. The QCM-D monitoring in real time of the XG adsorption on CNC spin-coated quartz crystals was performed at different XG concentrations (Fig. 1). This procedure allowed us to examine the kinetic deposition of XG on the cellulose surface.

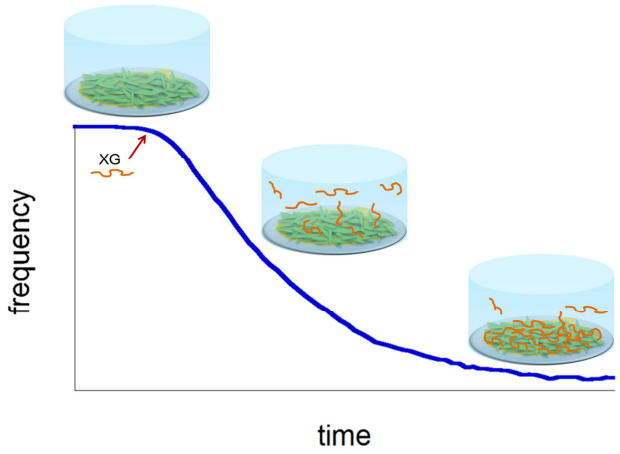

Fig. 1 Schematic illustration of XG adsorption onto spin-coated CNC surfaces monitored by quartz crystal microbalance.

The obtained results were discussed in terms of kinetic parameters of the association between XG and CNC that confirmed the presence of different regimes of XG adsorption. The adsorption of XG and other hemicelluloses onto cellulose has been previously studied by QCM-D[22, 23] but, to the best of our knowledge, this is the first kinetic study reported for the XG adsorption onto CNC surfaces.

Materials and methods

Materials

Cellulose nanocrystals (CNC) were prepared according to the method of Revol et al.[24] with minor modifications.[10] CNC were dispersed at 3 g L^{-1} in deionized water (18.2 MΩ, Millipore Milli-Q purification system). Xyloglucan (XG, M_W = 202 000 g mol^{-1}) from *Tamarindus indica* was provided by Megazyme (Ireland). Aqueous XG solutions (0.01-20 µg mL^{-1}) were prepared with deionized water. The structural features of XG are well described in literature.[16]

Surface preparation

Gold-coated quartz crystals and silicon wafers were cleaned in piranha solution H_2SO_4/H_2O_2 (7:3, v/v), rinsed exhaustively with Milli-Q water, and dried under a stream of nitrogen. Prior

to use, QCM-D quartz sensors were subjected to a plasma etching device (Harrick Plasma). Surfaces of CNC were prepared by the spin-coating method as previously described.[10, 25] CNC dispersion was dropped on a pre-coated substrate with poly(allylamine hydrochloride) (PAH) at 4 g L^{-1} in water and, after 5 min of adsorption, accelerated at 180 rpm s^{-1} to 3600 rpm for 60 s.

Surface characterization

Surface morphology of nanocrystals was studied by transmission electron microscopy (TEM). Nanocrystals suspensions in water were deposited on freshly glow-discharged carbon-coated electron microscope grids (200 mesh, Delta Microscopies, France) and the excess of water was removed by blotting. The sample was then immediately negatively stained with uranyl acetate solution (2%, w/v) for 2 min and dried after blotting. The grids were observed with a Jeol JEM 1230 TEM at 80 kv.

Topographical images on silicon wafers were registered by atomic force microscopy (AFM) by an Innova AFM (Bruker). The images were collected in tapping mode under ambient air conditions (temperature and relative humidity) using a monolithic silicon tip (TESPA, Bruker) with a spring constant of 42 N m^{-1}, and a nominal frequency of 320 kHz. Image processing was performed with the WSxM 5.0 software.

Film thickness was measured using a variable-angle spectroscopic ellipsometer (M-2000U; J.A. Woollam, Lincoln, USA). The ellipsometric angles, Δ and Ψ, were acquired over the spectroscopic range 250 – 1000 nm at three angles of incidence 65, 70 and 75°. Average thickness values were obtained from the measurement of at least 6 spots per film. Optical modeling and data analysis were performed using the CompleteEASE software package (J.A. Woollam Co., Inc.) using a three-layer model consisting on the Si(100) substrate, a thin SiO_2

layer, and the single Cauchy layer describing the nanocrystal layer and taking into account the surface roughness (~5 nm).

Quartz crystal microbalance with dissipation (QCM-D) experiments

QCM-D was used for both the determination of the water content of CNC layers and the XG adsorption onto CNC surfaces. QCM-D experiments were carried out with a Q-Sense E4 instrument (AB, Sweden) using a piezoelectric AT-cut quartz crystal coated with gold electrodes on each side (QSX301, Q-Sense). CNC surfaces were previously spin-coated onto the quartz crystal substrates and then placed in the QCM-D cells at 20ºC. Frequency ($\Delta f_n/n$) and (ΔD_n) dissipation changes were simultaneously registered at 5 MHz fundamental resonance frequency and its several overtones as a function of time. The third overtone (15 MHz) was used in the evaluation of the QCM-D data. The surface concentration (Γ) can be deduced from the frequency change ($\Delta f_n/n$) by using the Sauerbrey's equation:[26]

$$\Gamma = -C \frac{\Delta f_n}{n} \qquad (1)$$

where C is the constant for the mass sensitivity of the quartz crystal (0.177 mg m^{-2} Hz^{-1} for 5 MHz crystal), and n is the overtone number.

Determination of water content (or solvent fraction)

The water mass, Γ_{water}, associated to the nanocrystal layers was estimated by the H_2O/D_2O solvent exchange procedure monitored by QCM-D.[27, 28] CNC spin-coated layers were first allowed to swell in water for 2 h at a flow rate of 100 µL min^{-1} until the resonance signal was stable. Then, frequency and dissipation signals were offset to zero and deuterated water was introduced into the flow cell at a rate of 100 µL min^{-1}. After 10 min, water was again injected into the cell and the frequency returned to the initial baseline. From the differences in the frequency changes between the bare quartz crystals $(\Delta f_n/n)_{bare}$ and the CNC layer $(\Delta f_n/n)_{film}$,

the drop in frequency due to the water content $(\Delta f_n/n)_{water}$ can be calculated according to the following expression:[27]

$$\left(\frac{\Delta f}{n}\right)_{water} = \frac{\left(\frac{\Delta fn}{n}\right)_{film} - \left(\frac{\Delta fn}{n}\right)_{bare}}{\left(\frac{\rho_{D_2O}}{\rho_{H_2O}}\right) - 1} \quad (2)$$

where $(\Delta f_n/n)_{film}$ and $(\Delta f_n/n)_{bare}$ are the frequency changes observed when D_2O is introduced into the cell for the film and the bare quartz substrate, respectively, n the overtone number, and ρ_{D2O} and ρ_{H2O} the densities of deuterated and hydrogenated water, respectively. The water surface concentration, Γ_{H2O}, is then calculated from $(\Delta f_n/n)_{water}$ using the Sauerbrey's equation (Equation 1).

Adsorption isotherms of xyloglucan onto CNC surfaces

Spin-coated CNC surfaces were placed in the QCM-D cells at 20ºC and rinsed with water until the resonance response was stable. Then, frequency and dissipation signals were offset to zero just before the measurement. Xyloglucan solutions at different concentrations (0.01-20 µg mL^{-1}) were injected at 50 µL min^{-1} and allowed to adsorb for 40 min. Water was then injected in order to remove any loosely bound material. Each XG concentration was adsorbed on a freshly prepared CNC modified surface and the experiments were repeated at least three times.

The time evolution of XG adsorption onto cellulosic surfaces can be described by the Langmuir kinetic model which, in the absence of desorption, is expressed as:

$$\frac{d\theta}{dt} = k\,\beta(1-\theta) \quad (3)$$

In this equation, θ is defined as the fractional coverage, that is the ratio between the number of XG molecules adsorbed, N_{ads}, and the maximum number of XG molecules that can be adsorbed on the surface, N_{max}, ($\theta = N_{ads}/N_{max}$); β is the fractional initial concentration, that is

the ratio between the initial number of XG molecules, N_0, and the maximum number of XG molecules that can be adsorbed on the surface, N_{max}, ($\beta = N_0 / N_{max}$); and k is the kinetic constant.[29] In this expression, β can be considered constant so that the fraction of polymer available in solution will be $\beta - \theta$. Kinetics of adsorption can be therefore described by the following expression:

$$\frac{d\theta}{dt} = k\,(\beta - \theta)\left(1 - \frac{\theta}{\theta_e}\right) \qquad (4)$$

In this equation, θ_e is the fractional coverage at the equilibrium, that is the ratio between the number of XG molecules adsorbed at the equilibrium, $N_{e,ads}$, and the maximum number of XG molecules that can be adsorbed on the surface, N_{max}.

Results and Discussion

Surface characterization of nanocrystals layers

Micrographs from transmission electron microscopy (TEM) (Fig. 2a) on dried CNC surfaces showed nanocrystal average dimensions of 175±25 nm in length and 15±5 nm in width, which corresponded to an aspect ratio of 11.7, according to previously described cellulose nanocrystals from cotton.[2, 30] Comparatively, results from small angle neutron scattering (SANS) measurements have elucidated the form factor of the same CNCs in suspension. The curve, analysed with a form factor of a parallelepiped with a rectangular section, led to dimensions of 195±35 nm in length, 22±3 nm in width, and 6±0.2 nm in thickness,[31] which corresponded to aspect ratio of 8.9.

Morphology of CNC surfaces was also studied by AFM, in order to get more insight into the polymer surface available for XG adsorption in terms of roughness, molecular arrangement and surface coverage. For AFM studies, one layer of CNC was deposited onto silicon wafers by spin-coating. Fig. 2b shows the topographical images of CNC monolayer film and the representative cross-sectional profiles of the surface. AFM images revealed that the surface

was almost completely covered by the randomly distributed rod-like nanocrystals. The roughness of the CNC layer was calculated as the root mean squared (RMS) roughness and the obtained value was 6.2 nm. The thickness of the CNC layer, evaluated by ellipsometry, was 8.7±5.1 nm, which agreed with the thicknesses previously reported for cellulose layers (6-8 nm).[10, 17]

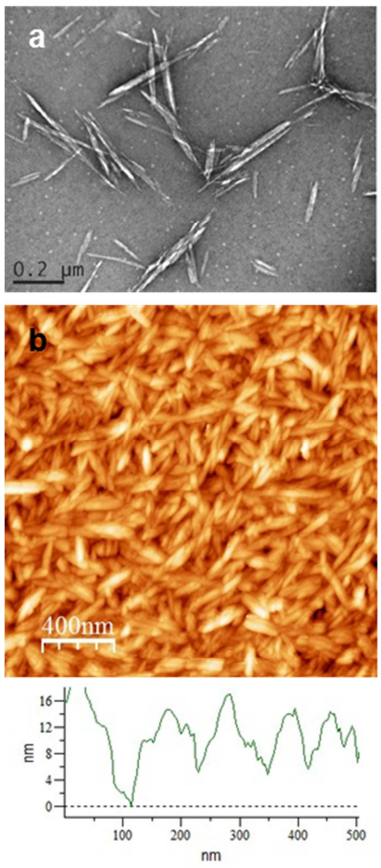

Fig. 2 TEM micrograph of negatively stained cellulose nanocrystals (a), and representative 2 × 2 µm^2 AFM topographical image of the spin-coated one-layer film of CNC at 3 g L^{-1} (b) onto a silicon wafer.

In order to quantify the surface concentration of the CNC film, a single layer of nanocrystals was deposited by spin-coating onto a gold-coated quartz crystal and the frequency was registered by QCM-D. The difference between the frequency of the bare quartz substrate and the nanocrystal coated quartz substrate allowed the calculation of the surface coverage by

using the Sauerbrey's equation (see Experimental section). The calculated surface concentration of the CNC monolayer was Γ_{CNC} = 18.71 mg m^{-2}. In an attempt to obtain more information into the CNC surface, the water content as an estimation of the void volume in the layer was determined by the H_2O/D_2O solvent exchange procedure monitored by QCM-D. This method permits the calculation of the solvent fraction within the film from the differences in the resonant frequency caused by the introduction of a deuterated solvent.[27] Fig. 3 shows the change in frequency ($\Delta f_n/n$) versus time t for a bare quartz crystal surface and for CNC surface switched from H_2O to D_2O and back to H_2O.

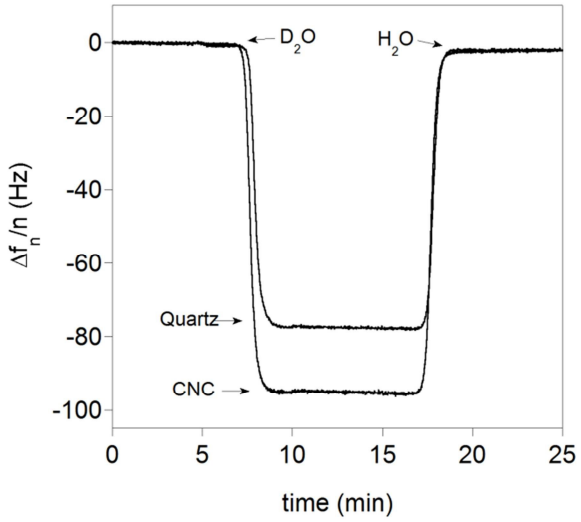

Fig. 3 Representative H_2O/D_2O solvent exchange frequency data of a bare gold-coated quartz crystal, and the one-layer CNC (3 g L^{-1}) film for the overtone number n = 3.

The difference in $\Delta f_n/n$ between the nanocrystal surface and the bare gold substrate was used to determine the frequency change due to the water uptake of CNC surface, according to Equation 2. The water mass uptake was then calculated by the Sauerbrey's expression (Equation 1). Thus, the D_2O content was estimated to be 25.0 mg m^{-2} for the CNC layer. This result agreed with those obtained by Kittle et al.[27] of 25-27 mg m^{-2} for both sulfated and desulfated cellulose nanocrystals films with a layer thickness of 7-9 nm. The H_2O/D_2O solvent exchange can be viewed as an estimation of the swelling extent and the void volume

within the nanocrystal films. In aqueous media, the pores will be "firstly" filled with water and subsequently replaced by deuterated water and concomitantly the layers will swell. Knowing the mass surface concentration of CNC, this corresponds to 134% water by mass within the CNC layer. As water does not penetrate the nanocrystals, the calculated water content must arise from surface porosity. This result, together with the AFM images, evidenced the roughness of CNC layers.

Adsorption of XG onto CNC surfaces

As the AFM images showed and confirmed the H_2O/D_2O solvent exchange experiments, CNC layers were rather rough surfaces so that XG molecules could not only adsorb on the surface but also partially penetrate the layer, which would increase the available surface for adsorption. The ability of XG to adsorb onto CNC surfaces confined as a thin layer was studied by quartz crystal microbalance with dissipation. QCM-D is powerful technique to probe polymer adsorption and associated water. It also gives information about the mechanical properties of the adsorbed layers through the dissipation changes. Furthermore, as the adsorption process is monitored *in situ*, kinetic parameters can be extracted from the QCM-D data. CNC surfaces were prepared onto gold-coated quartz crystals by the spin-coating technique. As the D_2O solvent exchange results showed, nanocrystals strongly swelled in aqueous media; therefore, CNC layers were firstly stabilized in water for 1 h in order to avoid the mass overestimation as a consequence of the water uptake by the CNC film. Once frequency and dissipation signals reached a constant value, they were offset to zero and XG solutions at different concentrations (0.01-20 μg mL^{-1}) were injected in a continuous flow mode. Fig. 4 shows the variations of frequency and dissipation for the overtone number n = 3 after the injection of XG on the spin-coated surfaces of CNC. For each XG concentration, a freshly prepared nanocrystal surface was employed; in Fig. 4, data arisen from some XG

concentrations have been removed for better visualization, they are shown in Supporting Information (Figure S1).

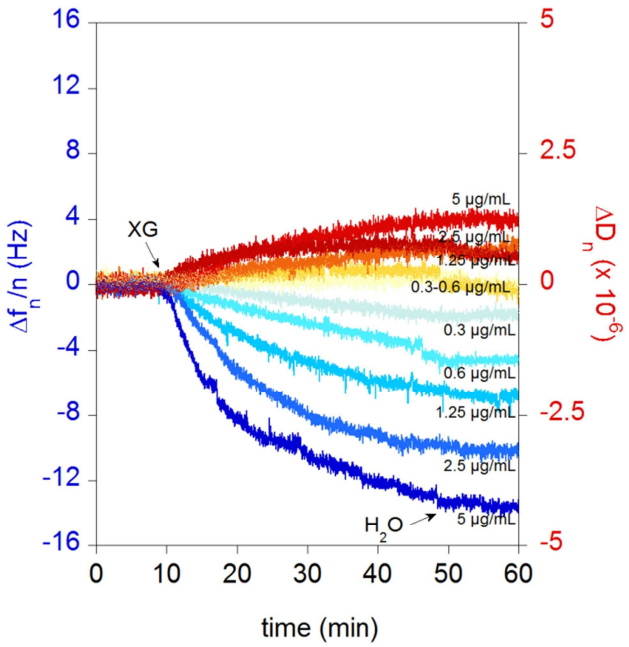

Fig. 4 Normalized frequency ($\Delta f_n/n$) and dissipation (ΔD_n) changes for the overtone number n = 3 of the CNC surface exposed to XG aqueous solutions at different concentrations (0.3-5 µg mL^{-1}) as a function of time. The arrows indicate where XG is injected and the rinse step with water.

No change in frequency or in dissipation was detected for XG concentrations below 0.3 µg mL^{-1}. Above this concentration, the graph clearly showed a decrease of the frequency signal after exposition to XG, which evidenced the adsorption of XG mass on the nanocrystals surface. It must be noted that for all XG concentrations, distinct frequency values were obtained despite a sufficient supply of XG from the continuously flushed with XG solution. This indicated that, especially at low XG concentrations, no further adsorption occurred that could lead to oversaturate the CNC layer, demonstrating the specific adsorption of XG onto CNC.

In addition to the adsorbed mass, QCM-D registers the dissipation changes as XG adsorption occurs. The dissipation value depends on the viscoelastic properties and also gives an indication about the hydration level of the layer. When the surfaces were exposed to XG, the dissipation signal remained close to zero. The negligible variation in CNC surface suggested a strong interaction and affinity of XG to the CNC surface[32] and minute modification of the rigid layer structure. Similar low dissipation values have been previously observed for the adsorption of XG onto cellulose nanofibrils.[33]

Possible unspecific adsorption of XG onto PAH pre-coated gold substrates or bare gold surfaces was discarded since the injection of XG resulted in negligible changes in frequency and dissipation regarding to changes observed for the CNC surfaces, which again suggested the specificity of XG to cellulosic surfaces. On the other hand, once XG was adsorbed onto the nanocrystals surface, the rinsing step with water did not produce desorption of xyloglucan molecules since no further frequency change was detected. The end of the binding event was assessed when the injection of XG solutions at increasing concentrations did not produce higher frequency drops. At a XG concentration of 5 µg mL^{-1} and above this concentration, $\Delta f_3/3$ reached -13.8 Hz and ΔD_3 reached $1.3 \cdot 10^{-6}$ units.

In Fig. 4, below 5 µg mL^{-1}, the XG adsorption at different concentrations did not result in the same frequency decrease at the end of the adsorption experiment. The frequency changes are proportionally related to the surface concentration, according to the Sauerbrey's equation (Equation 1); therefore, results indicated that increasing XG concentration resulted in higher amounts of XG adsorbed. This fact evidenced that XG adsorption was not thermodynamically but kinetically controlled over the time scale of the adsorption experiments. Often, adsorption isotherms may resemble to equilibrium isotherms; however, it is possible that these systems have not reached the steady state.[34] The adsorption of XG onto cellulosic surfaces has previously demonstrated to be rather slow and equilibrium may be not reached over 4 hours.[33]

In dispersed media, Langmuir model has been commonly used for the study of XG adsorption onto cellulosic surfaces, and maximum adsorption capacities from 98 to 333 $\mu g_{XG}\ m_{cellulose}^{-1}$ have been reported for crystalline cellulose.[35-39] However, other authors have pointed out that the Freundlich model is more appropriate to describe the binding of xyloglucan onto cellulose surfaces.[40, 41] In our experiments at the CNC surface, the different frequency values obtained after 40 minutes of adsorption for each XG concentration clearly evidenced that the equilibrium was not attained. In this situation, nor the Langmuir nor the Freundlich adsorption models can be used for describing the isotherms; therefore, the evolution with time of XG adsorption onto CNC surfaces will be studied in terms of an adsorption kinetic model. The kinetics of polymer adsorption is commonly described by a two-stage process.[42-44] Firstly, at low XG concentration or short adsorption time, every XG molecule reaching the uncovered CNC surface is directly adsorbed and has time to rearrange before new molecules arrive likely as monolayer or pancake conformation. Due to the surface availability, interactions between the XG chains are low. Initial adsorption is mainly limited by the diffusion of XG chains to the surface while internal chain rearrangement during adsorption is rather fast. Secondly, at longer times, when certain coverage is reached, the preformed layer can limit further molecules to adsorb on the surface due to steric hindrance and unavailability of binding sites. At the surface, interactions between XG chains become important and rearrangement in the layer becomes a limiting factor for adsorption.[42] Therefore, the overall adsorption process can be described as the contribution of the XG adsorption onto the uncovered CNC surface, and the contribution of the adsorption onto pre-covered CNC surfaces after XG rearrangement.[45-47] At low polymer concentrations, the surface coverage will be low so that polymer molecules can rearrange freely. In contrast, at higher concentrations, the coverage will be high and the polymer has no possibility to laterally rearrange. The model describing the kinetics of adsorption (Equation 4) can be expressed as the sum of the contribution of the adsorption onto

uncoated surfaces and the contribution of the adsorption onto pre-covered surfaces. The former contribution is the classical adsorption process whereas the later will take into account the rearrangement of deposited molecules. The kinetics of deposition will be therefore described by the following expression:[46]

$$\frac{d\theta}{dt} = k_1\,(\beta - \theta)\left(1 - \frac{\theta_1}{\theta_{e,1}}\right) + \; k_2\,\left(\frac{\theta_1}{\theta_{e,1}}\right)(\beta - \theta)\left(1 - \frac{\theta_2}{\theta_{e,2}}\right) \qquad (5)$$

In this model, the subscript 1 refers to a fast adsorption step onto uncovered CNC surface related to the transport of chains to the surface and fast mass deposition. The subscript 2 refers to the slower adsorption step onto pre-covered surface, which may be related to the internal reorganization of polymer chains. Therefore, k_1 and k_2 can be viewed as the kinetic constants for the adsorption onto uncovered surfaces revealing the affinity of both biopolymers, and for the rearrangement and adsorption onto pre-covered surfaces, respectively. If we assume that the coverage ratio θ_1 reaches a constant value on a relative short time scale, the expressions for the adsorbed XG are:

$$\theta_1 = \frac{1 - e^{k_1\left(1 - \frac{\beta}{\theta_{e,1}}\right)t}}{\frac{1}{\theta_{e,1}} - \left(\frac{1}{\beta}\right)e^{k_1\left(1 - \frac{\beta}{\theta_{e,1}}\right)t}} \qquad (6)$$

$$\theta_2 = \frac{1 - e^{k_2\left(1 - \frac{(\beta - \theta_{e,1})}{\theta_{e,2}}\right)t}}{\frac{1}{\theta_{e,2}} - \left(\frac{1}{\beta - \theta_{e,1}}\right)e^{k_2\left(1 - \frac{(\beta - \theta_{e,1})}{\theta_{e,2}}\right)t}} \qquad (7)$$

These expressions allow the calculation of the kinetic constant associated with the adsorption onto uncovered CNC surfaces, k_1, and the kinetic constant resulting from the adsorption after rearrangement of XG molecules, k_2. Desorption process was not taken into account in Equation 5 because the adsorption of XG onto cellulosic surfaces has been previously demonstrated to be irreversible.[22, 48] Indeed, QCM-D experiments have shown that XG was not desorbed from CNC surfaces over time or after the rinsing step (Fig. 4). The experimental fractional coverage values as a function of time, and the theoretical curves calculated by the

best fit of the kinetic model (Equation 5) from the different XG concentrations are shown in Fig. 5.

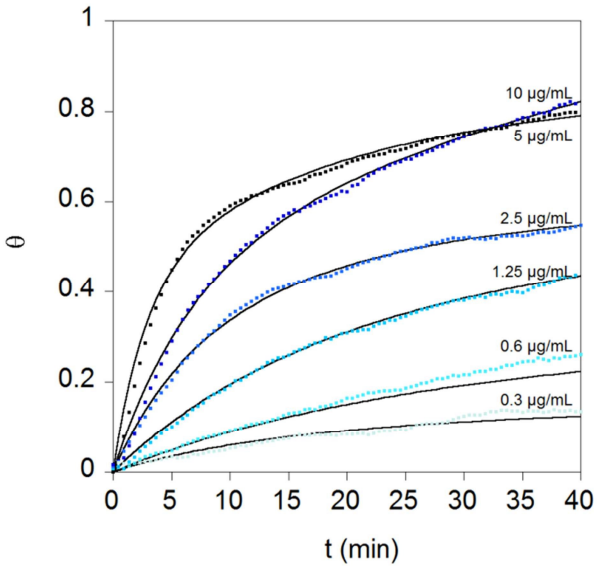

Fig. 5 Fractional XG coverage onto CNC surfaces as a function of time for the different XG concentrations studied (0.3-10 µg mL^{-1}). The squares correspond to experimental data and the solid lines represent the fit to Equation 5.

From Fig. 5, one can see that there is a good fit between the theoretical prediction (Equation 5) and the measured results for all XG concentrations evaluated. Moreover, above 5 µg mL^{-1} θ seemed to converge towards a similar value, confirming that XG adsorption onto the CNC layer was complete at concentrations around 5 µg mL^{-1}. This model assumes similar kinetic behavior for both contributions (adsorption and rearrangement) and allows the calculation of the apparent kinetic constants for the XG adsorption onto uncovered CNC surfaces, k_1, and for the adsorption after XG rearrangement, k_2 (Figures S2 and S3). Graphs showed that above a certain XG concentration (3.5 µg mL^{-1}), k_1 starts to increase slightly whereas k_2 clearly decreases. The ratio between k_1 and k_2 as a function of XG concentration is plotted in Fig. 6.

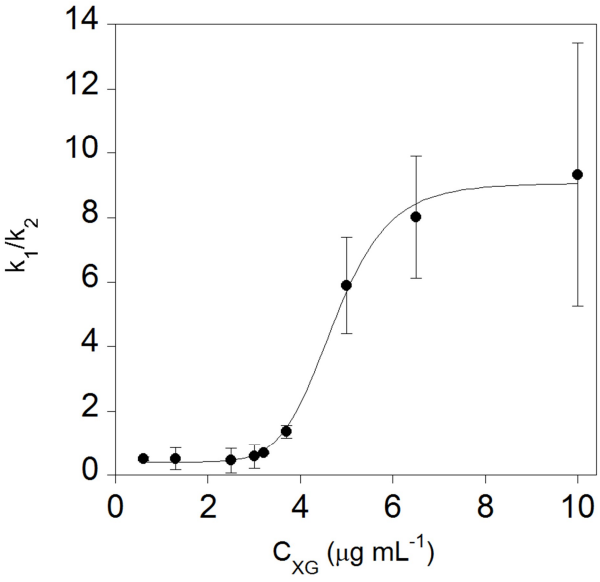

Fig. 6 Values of the ratio between the kinetic constant for adsorption onto uncovered CNC surfaces and the kinetic constant for adsorption after rearrangement, k_1/k_2, as a function of XG concentration.

At low XG concentrations (< 3.5 μg mL^{-1}), the k_1/k_2 ratio was lower than unit, which indicated that the adsorption after rearrangement was faster than the adsorption onto uncovered CNC surfaces. Differently, when XG concentration increased (> 3.5 μg mL^{-1}), the k_1/k_2 ratio became gradually greater, with a kinetic constant for the adsorption onto the uncovered CNC surface, k_1, up to more than eight times higher than the kinetic adsorption constant for rearrangement, k_2. These data confirmed the presence of two adsorption regimes for the XG adsorption onto CNC surfaces, as we have already stated.[38] Previous studies performed by us revealed that at dilute concentrations XG is not accessible to enzymatic degradation suggesting that XG chains adsorb on CNC in a rather flat conformation with a high percentage of trains in close contact with cellulose surface that cannot be hydrolyzed by xyloglucanase.[38] More than 85% of the XG chains were found to be inaccessible and thus likely adsorb as trains. This point is in good agreement with the low k_1/k_2 ratio that evidenced a rearrangement of XG chains onto CNC surfaces. In contrast, as XG concentration increases,

the percentage of loops and tails gradually rises from 15% to an average value of 48%.[38] This concentrated regime is indicative of CNC surface saturation. At this point, k_1/k_2 ratio is high and adsorption kinetics is fast. Loops and tails of XG do not have time to laterally rearrange to a flat conformation before new XG molecules adsorb. Loops and tails are not really adsorbed on the surface but stretched out away, which fully coat the surface and prevent penetration into the initial layer. Therefore, new XG molecules adsorb in a more compact conformation leading to gradually denser layers containing kinks, loops and mushroom conformation.

In the early stages of adsorption, the XG deposition on the CNC surface can be described as a diffusion-controlled process. The diffusion coefficient toward the surface can be related to the adsorbed amount by the following expression derived from Fick's law:[42, 49]

$$\Gamma = 2\, C_{XG}\sqrt{\frac{D_{surf}t}{\pi}} \qquad (8)$$

In this equation, Γ is the surface concentration in mg m^{-2}, C_{XG} is the XG concentration in solution (µg mL^{-1}), D_{surf} is the diffusion coefficient of XG toward the surface (cm^2 s^{-1}), and t is the time (s^{-1}). The diffusion coefficient toward the surface may differ from the diffusion coefficient in solution because D_{surf} include the contribution of interactions between the polymer and the surface, which may influence interfacial adsorption.[49] Fig. 7 plots the adsorbed amount of XG as a function of the square root of the adsorption time.

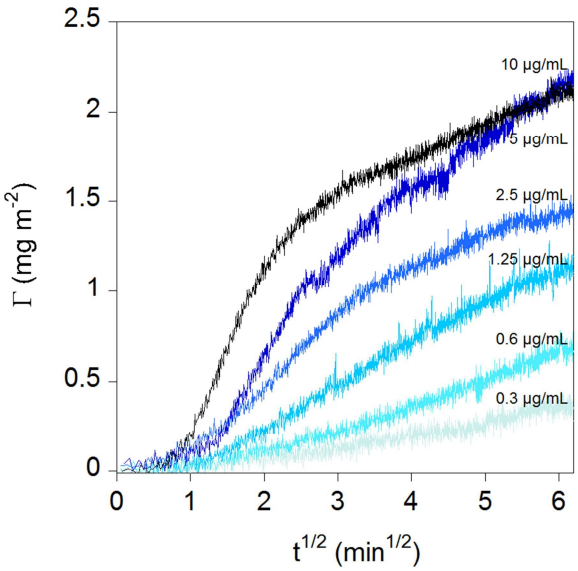

Fig. 7 Amount of XG adsorbed onto CNC surface as a function of the square root of the adsorption time for the different XG concentrations (0.3-10 µg mL^{-1}).

The graph clearly shows a Fickian behavior for all XG concentrations studied since the mass change rate is proportional to the square root of the time. The agreement of experimental data to the Fickian diffusion-limited model is depicted in Fig. 8:

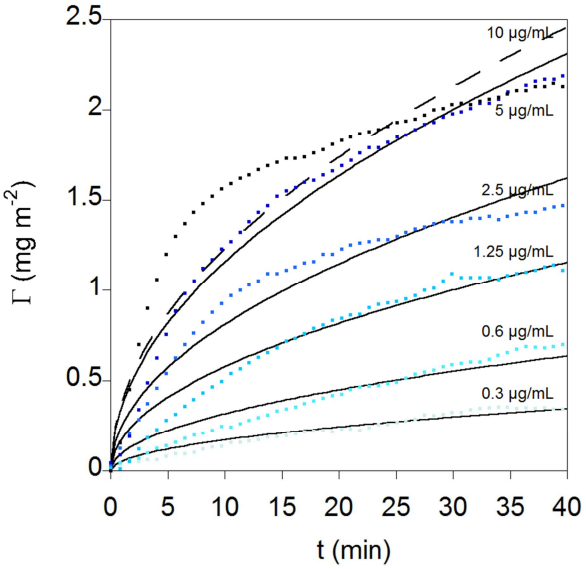

Fig. 8 Profiles of kinetics of adsorption of XG onto CNC surfaces for the different XG concentrations studied (0.3-10 µg mL^{-1}). The squares correspond to the experimental data,

and the solid black lines are the fitting results obtained using the Fickian diffusion-limited model. For better visualization, fitting for the highest XG concentration (10 µg mL^{-1}) has been depicted in dashed line.

The plot clearly shows good fits at low XG concentrations whereas deviation was found for the higher concentration (10 µg mL^{-1}). These results evidenced the Fickian behavior for concentrations below 10 µg mL^{-1}. In this diffusion-limited regime, it is possible to determine a diffusion coefficient of XG toward the surface from the slope of the adsorbed amount versus the square root of time curve (Fig. 7), according to Equation 8. At high XG concentrations, where the graph of the amount of XG adsorbed versus squared time showed two slopes, the diffusion coefficient was calculated from the slope of the steepest part corresponding to the initial stages of adsorption. These values are depicted in Fig. 9 as a function of the XG concentration.

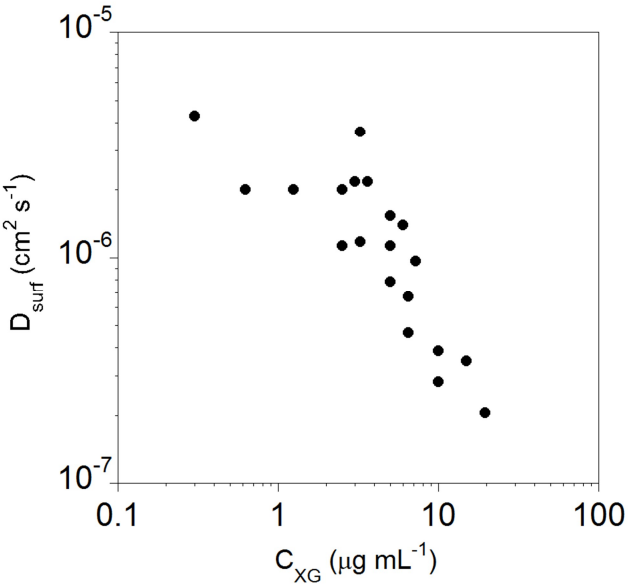

Fig. 9 Diffusion coefficient (cm^2 s^{-1}) of XG onto the CNC surface as a function of XG concentration (µg mL^{-1}) in logarithmic scale.

The D_{surf} values decreased with increasing concentration from 3.3 10^{-7} cm^2 s^{-1} for XG at 10 µg mL^{-1} to 4.3 10^{-6} cm^2 s^{-1} at 0.3 µg mL^{-1}. This behavior has been previously observed,[49, 50] and it could be explained in terms of the slower diffusion of XG chains at concentrated regimes. On one hand, increasing concentration favors intermolecular interactions between XG chains, resulting in partially aggregated XG molecules with lower diffusion rates. On the other hand, at concentrated regimes, XG rapidly adsorbs onto the CNC surface so that the presence of this XG layer may slow down further XG diffusion to the surface.

From these data, we propose a model for XG binding onto nanocrystal film surfaces. It is assumed that the β-(1-4)-linked backbones of XG and cellulose interact by hydrogen bonds and van der Waals interactions, and the system is stabilized by interactions with the XG side chains.[48] The presence of side chains in the XG structure provides flexibility allowing polymer mobility in solution and its rearrangement after adsorption on the CNC surface. At the beginning of the adsorption process, it can be assumed that every XG molecule reaching the surface is directly adsorbed. XG configuration would be determined by the initial contact with CNC, which is usually the result of the XG collisions with the surface. Initially, the XG conformation on the cellulosic surface will be similar to the conformation in solution.[51] After contact is made, changing the XG conformation involves breaking and establishing interactions between polysaccharide segments and surface sites. According to the two-stage model, the arrangement of chains at the surface to adopt a favorable conformation for adsorption is fast compared to the necessary diffusion times.[52-54] At very dilute regimes, below 3.5 µg mL^{-1}, XG will rearrange until forming a tightly anchored layer (trains) with all sugar residues interacting with the CNC surface. The surface coverage is still low and XG molecules have still available sites for adsorption. Differently, at more concentrated regimes, over a critical concentration of 3.5 µg mL^{-1}, even at the early stages of adsorption, new XG molecules reach the surface before the former can rearrange and XG will be maintained in the

vicinity of the surface with segments extending more or less into the liquid phase (loops, tails or mushrooms). At this point, neighboring adsorbed polymers can interfere with this rearrangement and slow it down. Fig. 10 shows a schematic description of the two regimes of XG adsorption.

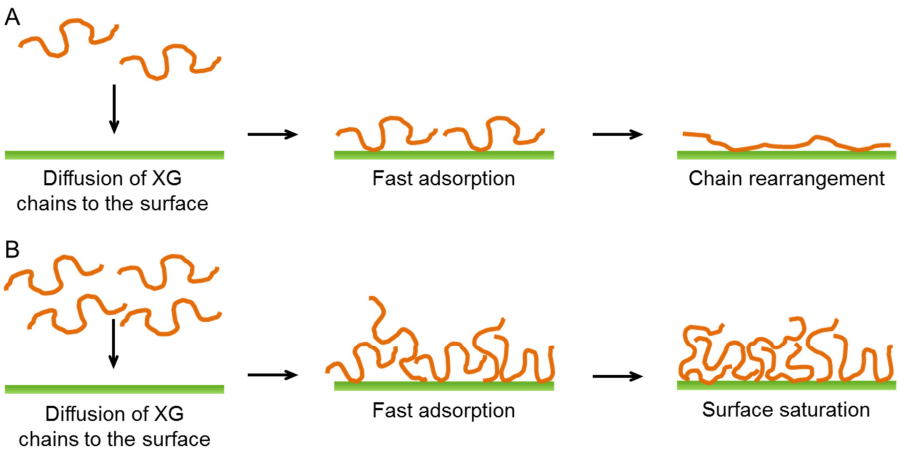

Fig. 10 Schematic description of XG adsorption onto CNC surfaces at very diluted (A) and more concentrated (B) XG regimes.

In this article, we have used a kinetic model that separates the contribution of adsorption and the effect of rearrangement. To the best of our knowledge, this is the first time the adsorption of xyloglucan onto cellulose has been described in terms of kinetic parameters. Our study reports the occurrence of two XG adsorption regimes on cellulose surface. This finding can provide a mean to get a better insight into the biological role of XG. Indeed, these results in combination with our previous ones[35-39] suggest that XG can be present according to two types of conformations when adsorbed on cellulosic surfaces. At low concentration the rearrangement process of XG chains on the surface is faster than further adsorption of XG. We have previously demonstrated that, in this regime, XG chains are not susceptible to enzymatic hydrolysis suggesting that they are in close contact with the cellulose chains [35-39]. It can be thus concluded that XG is mainly arranged as chains lying flat on the surface and can create a tight association between two cellulose surfaces. Such assemblies have been proposed

by Park et al. [55] as an element for the mechanical properties of the plant cell wall. Hence, low initial amount of XG in the cell may favor highly efficient cross-link between cellulose fibrils. On the contrary, at higher XG concentration, adsorption is faster than rearrangement and thus XG forms a “fluffy carpet” conformation composed of trains, loops and hairpins onto cellulose.[34] This arrangement can provide steric hindrance that can help to the slippery effect observed when cellulose surface is coated with XG.[10-12, 17, 18, 56]

Conclusions

Adsorption isotherms of XG on CNC fixed at a surface by spin-coating were used to get more insight into the molecular arrangement of the association between XG and CNC. Kinetic studies of QCM-D data evidenced the presence of two adsorption regimes, and allowed to propose a model for describing the XG adsorption on cellulosic surfaces. Hence, at very dilute XG concentrations, after adsorption, XG molecules have time to rearrange resulting in a flat conformation forming essentially trains onto the cellulosic surface. Differently, at higher XG concentrations, the XG adsorption onto CNC results in the formation of a higher percentage of loops and tails that rapidly cover the CNC surface with a dense layer of XG that prevents rearrangement. Thus, we propose that XG adsorption is governed by kinetic parameters rather than by thermodynamic equilibrium. Our study provides theoretical support to experimental results previously reported by our team and others. These results give more insight into the cellulose-xyloglucan organization and function in an attempt to understand the cell wall architecture and the physiological role of XG, which could also encourage the design of novel biomimetic materials. Moreover, it will also provide some theoretical tools for further studies that will aim to compare adsorption processes of structurally different hemicelluloses and thus may help to understand the functional roles of the broad biological variability of this biopolymer class.

Acknowledgements

Ana Villares has received the support of the European Union, in the framework of the Marie-Curie FP7 COFUND People Programme, through the award of an AgreenSkills' fellowship (under grant agreement n° 267196). We are grateful for the financial support from the MATIERES project funded by the "Région Pays de la Loire" council. The authors acknowledge the BIBS platform of INRA Angers-Nantes for the access to microscopy facilities. Nadège Beury and Emilie Perrin are acknowledged for the excellent technical support for the CNC preparation, characterization and microscopy analysis.

References

1. A. Dufresne, *Materials Today*, 2013, **16**, 220-227.
2. I. Capron and B. Cathala, *Biomacromolecules*, 2013, **14**, 291-296.
3. I. Kalashnikova, H. Bizot, P. Bertoncini, B. Cathala and I. Capron, *Soft Matter*, 2013, **9**, 952-959.
4. A. N. Nakagaito and H. Yano, *Applied Physics A - Materials Science & Processing*, 2004, **78**, 547-552.
5. Q. Wu, Y. Meng, K. Concha, S. Wang, Y. Li, L. Ma and S. Fu, *Industrial Crops and Products*, 2013, **48**, 28-35.
6. S. Belbekhouche, J. Bras, G. Siqueira, C. Chappey, L. Lebrun, B. Khelifi, S. Marais and A. Dufresne, *Carbohydrate Polymers*, 2011, **83**, 1740-1748.
7. J. George, K. V. Ramana, A. S. Bawa and Siddaramaiah, *International Journal of Biological Macromolecules*, 2011, **48**, 50-57.
8. C. Martin and J. Bruno, *Nordic Pulp and Paper Research*, 2014, **29**, 19-30.
9. C. Olivier, C. Moreau, P. Bertoncini, H. Bizot, O. Chauvet and B. Cathala, *Langmuir*, 2012, **28**, 12463-12471.
10. C. Cerclier, F. Cousin, H. Bizot, C. Moreau and B. Cathala, *Langmuir*, 2010, **26**, 17248-17255.
11. C. Cerclier, A. Guyomard-Lack, C. Moreau, F. Cousin, N. Beury, E. Bonnin, B. Jean and B. Cathala, *Advanced Materials*, 2011, **23**, 3791.
12. A. Dammak, C. Moreau, N. Beury, K. Schwikal, H. T. Winter, E. Bonnin, B. Saake and B. Cathala, *Holzforschung*, 2013, **67**, 579-586.
13. A. Hambardzumyan, M. Molinari, N. Dumelie, L. Foulon, A. Habrant, B. Chabbert and V. Aguie-Beghin, *Comptes Rendus Biologies*, 2011, **334**, 839-850.
14. F. Li, P. Biagioni, M. Finazzi, S. Tavazzi and L. Piergiovanni, *Carbohydrate Polymers*, 2013, **92**, 2128-2134.
15. Z.-D. Qi, T. Saito, Y. Fan and A. Isogai, *Biomacromolecules*, 2012, **13**, 553-558.
16. S. C. Fry, *Journal of Experimental Botany*, 1989, **40**, 1-11.
17. B. Jean, L. Heux, F. Dubreuil, G. Chambat and F. Cousin, *Langmuir*, 2009, **25**, 3920-3923.

18. H. T. Winter, C. Cerclier, N. Delorme, H. Bizot, B. Quemener and B. Cathala, *Biomacromolecules*, 2010, **11**, 3144-3151.
19. J. Gu and J. M. Catchmark, *Cellulose*, 2014, **21**, 275-289.
20. S. E. C. Whitney, M. G. E. Gothard, J. T. Mitchell and M. J. Gidley, *Plant Physiology*, 1999, **121**, 657-663.
21. B. S. Valent and P. Albersheim, *Plant physiology*, 1974, **54**, 105-108.
22. P. Eronen, K. Junka, J. Laine and M. Osterberg, *Bioresources*, 2011, **6**, 4200-4217.
23. P. Eronen, M. Osterberg, S. Heikkinen, M. Tenkanen and J. Laine, *Carbohydrate Polymers*, 2011, **86**, 1281-1290.
24. J. F. Revol, H. Bradford, J. Giasson, R. H. Marchessault and D. G. Gray, *Int. J. Biol. Macromol.*, 1992, **14**, 170-172.
25. A. Guyomard-Lack, C. Cerclier, N. Beury, B. Jean, F. Cousin, C. Moreau and B. Cathala, *European Physical Journal: Special Topics*, 2012, **213**, 291-294.
26. G. Sauerbrey, *Zeitschrift für Physik*, 1959, **155**, 206-222.
27. J. D. Kittle, X. Du, F. Jiang, C. Quian, T. Heinze, M. Roman and A. R. Esker, *Biomacromolecules*, 2011, **12**, 2881-2887.
28. J. D. Kittle, C. Wang, C. Qian, Y. Zhang, M. Zhang, M. Roman, J. R. Morris, R. B. Moore and A. R. Esker, *Biomacromolecules*, 2012, **13**, 714-718.
29. B. Alince, J. Petlicki and T. G. M. Vandeven, *Colloids and Surfaces*, 1991, **59**, 265-277.
30. I. Kalashnikova, H. Bizot, B. Cathala and I. Capron, *Biomacromolecules*, 2012, **13**, 267-275.
31. F. Cherhal, F. Cousin and I. Capron, *Langmuir*, 2015, **31**, 5596-5602.
32. D. E. Otzen, M. Oliveberg and F. Hook, *Colloids and Surfaces B-Biointerfaces*, 2003, **29**, 67-73.
33. S. Ahola, P. Myllytie, M. Osterberg, T. Teerinen and J. Laine, *Bioresources*, 2008, **3**, 1315-1328.
34. T. G. M. Van de Ven, *Advances in Colloid and Interface Science*, 1994, **48**, 121-140.
35. T. Hayashi, K. Ogawa and Y. Mitsuishi, *Plant and Cell Physiology*, 1994, **35**, 1199-1205.
36. M. Lopez, H. Bizot, G. Chambat, M.-F. Marais, A. Zykwinska, M.-C. Ralet, H. Driguez and A. Buleon, *Biomacromolecules*, 2010, **11**, 1417-1428.
37. J. Gu and J. M. Catchmark, *Cellulose*, 2013, **20**, 1613-1627.
38. A. Dammak, B. Quemener, E. Bonnin, C. Alvarado, B. Bouchet, A. Villares, C. Moreau and B. Cathala, *Biomacromolecules*, 2015, **16**, 589-596.
39. A. Bodin, L. Ahrenstedt, H. Fink, H. Brumer, B. Risberg and P. Gatenholm, *Biomacromolecules*, 2007, **8**, 3697-3704.
40. A. Zykwinska, J.-F. Thibault and M.-C. Ralet, *Carbohydrate Polymers*, 2008, **74**, 23-30.
41. C. Pirich, R. de Freitas, M. Woehl, G. Picheth, D. S. Petri and M. Sierakowski, *Cellulose*, 2015, **22**, 1773-1787.
42. H. Motschmann, M. Stamm and C. Toprakcioglu, *Macromolecules*, 1991, **24**, 3681-3688.
43. L.-E. Enarsson and L. Wagberg, *Langmuir*, 2008, **24**, 7329-7337.
44. B. O'Shaughnessy and D. Vavylonis, *Journal of Physics-Condensed Matter*, 2005, **17**, R63-R99.
45. L. Couture and T. G. M. Vandeven, *Colloids and Surfaces*, 1991, **54**, 245-260.
46. J. A. De Witt and T. G. M. Van de Ven, *Langmuir*, 1992, **8**, 788-793.
47. L. Wagberg, L. Odberg, T. Lindstrom and R. Aksberg, *Journal of Colloid and Interface Science*, 1988, **123**, 287-295.

48. J. Hanus and K. Mazeau, *Biopolymers*, 2006, **82**, 59-73.
49. K. Sakai, E. G. Smith, G. B. Webber, C. Schatz, E. J. Wanless, V. Butun, S. P. Armes and S. Biggs, *Journal of Physical Chemistry B*, 2006, **110**, 14744-14753.
50. H. Walter, C. Harrats, P. Muller-Buschbaum, R. Jerome and M. Stamm, *Langmuir*, 1999, **15**, 1260-1267.
51. L. Wagberg and R. Hagglund, *Langmuir*, 2001, **17**, 1096-1103.
52. E. Guzman, F. Ortega, N. Baghdadli, G. S. Luengo and R. G. Rubio, *Colloids and Surfaces A - Physicochemical and Engineering Aspects*, 2011, **375**, 209-218.
53. E. Guzman, H. Ritacco, F. Ortega and R. G. Rubio, *Colloids and Surfaces A - Physicochemical and Engineering Aspects*, 2011, **384**, 274-281.
54. E. Guzman, H. A. Ritacco, F. Ortega and R. G. Rubio, *Journal of Physical Chemistry C*, 2012, **116**, 15474-15483.
55. Y. B. Park and D. J. Cosgrove, *Plant Physiology*, 2012, **158**, 1933-1943.
56. J. Stiernstedt, H. Brumer, III, Q. Zhou, T. T. Teeri and M. W. Rutland, *Biomacromolecules*, 2006, **7**, 2147-2153.